



Numerical modelling of the thermal bar and its ecological consequences in a river-dominated lake

Paul R. Holland¹, Anthony Kay*, Vincenzo Botte

Department of Mathematical Sciences, Loughborough University, Loughborough, Leicestershire LE11 3TU, UK

Received 2 August 2002; accepted 2 July 2003

Abstract

Predictions from the first realistic model of the hydrodynamics of the riverine thermal bar in a medium-size lake are presented. Important features of field observations from Kamloops Lake, British Columbia are successfully reproduced, but the model adopts a generalised section, which is regarded as being representative of many other lakes. A study of the model sensitivity to various aspects of its formulation is also presented, particularly emphasising the important influence of Coriolis forcing on the thermal bar circulation. Plankton population dynamics within the thermal bar flow field is then studied by means of two ecological models of differing complexity. Differences between the predictions of the two models are explained with reference to intermediate simulations, and it is found that the simple ecosystem formulation used in previous work may give misleading results. The flow and stability conditions of the riverine thermal bar have a profound influence on ecosystem development, and support greater phytoplankton growth than in thermal bars resulting purely from radiative effects.

© 2003 Elsevier B.V. All rights reserved.

Keywords: Lake dynamics; Numerical analysis; Plankton; River plumes; Thermal bar

Regional terms: Canada; British Columbia; Kamloops Lake

1. Introduction

An important feature of the circulation of many lakes in temperate regions is the thermal bar, a downwelling plume of water that arises from the existence of a temperature of maximum density (T_{md}) in fresh water. The classical thermal bar appears in lakes in spring and autumn when the surface

temperature passes through the T_{md} due to radiative effects; near-shore shallow regions are affected first (since heating and cooling are fastest there) and a sinking plume of maximally dense water appears at the lake shore and migrates towards the deeper regions as the surface heat flux continues (Zilitinkevich et al., 1992).

Several field studies have shown that the thermal bar has an important influence upon effluent and nutrient distributions within temperate lakes, with the horizontal motions converging at the thermal bar limiting the water available for the dilution of near-shore releases by forming a barrier to horizontal transport (Moll et al., 1993; Gbah and Murthy, 1998). As a boundary between warm, stable, shallow

* Corresponding author. Tel.: +44-1509-222-878; fax: +44-1509-223-969.

E-mail address: a.kay@lboro.ac.uk (A. Kay).

¹ Present address: Centre for Polar Observation and Modelling, Department of Space and Climate Physics, University College London, Gower Street, London WC1E 6BT, UK.

waters and cool, isothermal, deep waters, the thermal bar also acts as an interface between favourable and less favourable conditions for plankton growth. Field observations by Likhoshway et al. (1996) of plankton population dynamics in the vicinity of the spring thermal bar of Lake Baikal in Siberia have been qualitatively reproduced by Botte and Kay (2000) (hereafter referred to as BK), using an ecosystem simulation based upon a simple biological formulation coupled to a full hydrodynamical model. These studies showed the horizontal motions converging at the thermal bar producing a localised plankton bloom. In addition, BK confirmed that plankton productivity is highly dependent upon vertical diffusion rates, as stable stratification of the water column suppresses vertical transport of biomass away from the photic zone and thus encourages continued growth.

In contrast to the classical case, the riverine thermal bar is generated at a river inflow where lake and river temperatures are on opposite sides of the T_{md} . In spring, a surface heat flux will warm a relatively shallow and rapidly mixed river through the T_{md} more rapidly than a deep lake, and conditions are then favourable for the formation of a thermal bar at the confluence of the two water masses. Due to the effects of dissolved and suspended matter transported by a river inflow, the influence of a riverine thermal bar on pollutant dispersion and ecosystem function is likely to be even more important than that of its classical counterpart. The differing properties of river and lake water mean that the spring riverine thermal bar forms a barrier between nutrient-rich and pollutant-rich, turbid, warm, and stable waters inshore of the T_{md} and relatively nutrient-limited, clear, cool, and isothermal conditions offshore (Ullman et al., 1998; Budd et al., 1999). Depending upon the exact balance of the river in question, this extra turbidity and effluent influx could either promote or suppress the favoured plankton growth inshore of and at the thermal front. The differences between the classical and riverine thermal bars in influence on plankton populations are currently unknown.

While several observed thermal bars are influenced slightly by riverine waters, detailed observations of a predominantly riverine thermal bar are only available for Kamloops Lake in British Columbia, Canada (Carmack, 1979; Carmack et al., 1979). The only previous model of the dynamics of the riverine

thermal bar is that of Holland et al. (2001), a study hereafter denoted HKB, who performed numerical simulations on a simple deep-lake section in a bid to assess the enhancement of vertical transport, which may be produced with a riverine salinity higher than that of the lake. There have been no previous attempts at realistically modelling the dynamics and propagation of the riverine thermal bar throughout the spring warming, and the phenomenon and its effects on the plankton ecosystem of a lake are poorly understood as a result.

This study seeks to remedy this lack of knowledge by elucidating the dynamical effects of the riverine thermal bar in a section nominally representative of Kamloops Lake, a long and thin temperate fjord-type lake. Situated immediately downstream of Kamloops City, within the coordinates 50:26–50:42°N and 120:03–120:32°W, Kamloops Lake appears as a widening of the through-flowing Thompson River (Fig. 1a), which totally dominates the lake's circulation and thermal regime (St. John et al., 1976). Kamloops Lake is important as a primary rearing

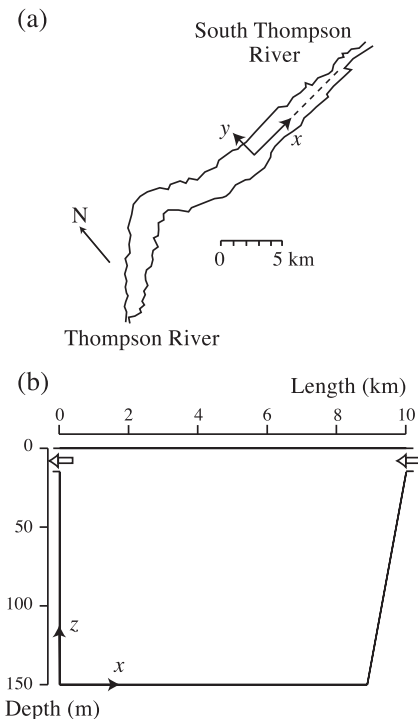


Fig. 1. (a) Outline of Kamloops Lake showing position of section and orientation of axes; (b) section bathymetry.

ground for three species of Pacific salmon: coho, chinook, and sockeye (Ward, 1964), and is en route for many adult salmon returning to upstream breeding areas, as well as smolts heading downstream to the Pacific Ocean. The lake was included as a major tributary in the recent 7-year Fraser River Action Plan, which was prompted by widespread concern over the health of British Columbia's waterways (Gray and Tuominen, 1999).

Kamloops Lake is surprisingly healthy given the historical discharge of pollutants into the Upper Thompson River, and this is partly due to circulations associated with the riverine thermal bar. Deep mixing of nutrients and effluents away from the euphotic zone prevents the in situ growth of harmful bacteria, which unfortunately tend to appear downstream instead (Killworth and Carmack, 1979). The riverine thermal bar of Kamloops Lake is therefore of great importance to the health of the Thompson River ecosystem as a whole.

To attain a basic first understanding of the riverine thermal bar and the influence of salinity, HKB were forced to neglect several important features, including Coriolis forces, surface heating, and a realistic bathymetry. In contrast to these assumptions, a review of thermal bar observations from a wide range of lakes suggests that the realism of the predicted flow field should depend upon resolving these factors (Holland, 2002). In particular, analytical studies of the thermal bar in a rotating frame have revealed that Coriolis forces are responsible for the 'thermal wind' flows parallel to the front that dominate observed circulations (Brooks and Lick, 1972; Huang, 1972). While a Coriolis-driven deflection of the inflowing river plume is observed in Kamloops Lake (Hamblin and Carmack, 1978; Carmack, 1979), the narrowness of the river delta limits the impact of this forcing.

The first aim of this paper is to reproduce the Kamloops Lake observations of Carmack (1979) and thereby understand the flow regime of the riverine thermal bar. The sensitivity of the riverine thermal bar to river salinity and the previously neglected factors mentioned above are then tested, so the present work may be viewed as both a validation of HKB and a first study of a realistic riverine thermal bar. The hydrodynamical simulation forms

the basis of a numerical study of the ecological effects of the riverine thermal bar, in two parts. Firstly, the simple ecosystem formulation of Franks et al. (1986) is used as it was in BK in order to elucidate the differing influences on plankton growth of the classical and riverine thermal bars. Secondly, the more sophisticated formulation of Parker (1991) is adopted, testing some of the assumptions underlying previous work. Unfortunately, while Kamloops Lake has the only published detailed physical data on the riverine thermal bar, data on its plankton are practically nonexistent in the literature. Our ecological modelling is therefore oriented towards only a qualitatively correct solution.

The layout of the paper is as follows. The hydrodynamical model is described in Section 2. Results from a reference simulation of the riverine thermal bar are given in Section 3, together with an investigation of various changes to the model formulation, determining the importance of salinity, Coriolis force, bathymetry, and surface heating. A similar pattern is then followed with regard to the ecological simulations: Section 4 describes the two plankton population models, Sections 5 and 6 give the results from the respective models, and Section 7 examines the sensitivity of ecosystem behaviour to each of the features that differ between the two models. Some overall conclusions are given in Section 8.

2. Dynamical model

Apart from the domain bathymetry, the physical model employed in this study is virtually identical to that adopted by HKB, and only a brief description is presented here.

In order to obtain the relatively fine spatial resolution required to model the thermal bar, a two-dimensional river delta section is adopted with the justification that gradients normal to the shore are much larger than those parallel to it. The latter are therefore neglected, while flow is still permitted in this direction. Cartesian coordinates x , y , and z are defined such that z represents the vertical direction, taken as positive upwards, x increases towards the river inflow, and y is perpendicular to the section, as shown in Fig. 1a and b.

The study employs a quasi-incompressible formulation of the Reynolds-averaged Navier–Stokes equations under the Boussinesq approximation, so that the density is taken to equal the maximum density of pure water at $p=0$, $\rho_c=999.975 \text{ kg m}^{-3}$, everywhere except in the buoyancy term. Under these assumptions, the continuity equation becomes:

$$\frac{\partial u}{\partial x} + \frac{\partial w}{\partial z} = 0 \quad (1)$$

and the components of the momentum equation are:

$$\begin{aligned} \frac{\partial u}{\partial t} + u \frac{\partial u}{\partial x} + w \frac{\partial u}{\partial z} = \frac{\partial}{\partial x} \left(A_h \frac{\partial u}{\partial x} \right) + \frac{\partial}{\partial z} \left(A_v \frac{\partial u}{\partial z} \right) \\ - \frac{1}{\rho_c} \frac{\partial p}{\partial x} + 2\Omega_z v - 2\Omega_y w \end{aligned} \quad (2)$$

$$\begin{aligned} \frac{\partial v}{\partial t} + u \frac{\partial v}{\partial x} + w \frac{\partial v}{\partial z} = \frac{\partial}{\partial x} \left(A_h \frac{\partial v}{\partial x} \right) + \frac{\partial}{\partial z} \left(A_v \frac{\partial v}{\partial z} \right) \\ + 2\Omega_x w - 2\Omega_z u \end{aligned} \quad (3)$$

$$\begin{aligned} \frac{\partial w}{\partial t} + u \frac{\partial w}{\partial x} + w \frac{\partial w}{\partial z} = \frac{\partial}{\partial x} \left(A_h \frac{\partial w}{\partial x} \right) + \frac{\partial}{\partial z} \left(A_v \frac{\partial w}{\partial z} \right) \\ - \frac{1}{\rho_c} \frac{\partial p}{\partial z} - \frac{\rho}{\rho_c} g + 2\Omega_y u \\ - 2\Omega_x v, \end{aligned} \quad (4)$$

where A_h and A_v are eddy viscosity coefficients in the horizontal and vertical directions, respectively; g is the acceleration due to gravity; and Ω_x , Ω_y , and Ω_z are the components of the Earth's angular velocity vector. Density is calculated from the [Chen and Millero \(1986\)](#) equation of state, which implicitly includes the influence of salinity on the T_{md} .

An equation for the transport of scalar quantities Φ is simply obtained by considering a balance between convection and diffusion:

$$\frac{\partial \Phi}{\partial t} + u \frac{\partial \Phi}{\partial x} + w \frac{\partial \Phi}{\partial z} = \frac{\partial}{\partial x} \left(K_h \frac{\partial \Phi}{\partial x} \right) + \frac{\partial}{\partial z} \left(K_v \frac{\partial \Phi}{\partial z} \right), \quad (5)$$

where K_h and K_v are diffusivity coefficients for the transported quantity in each coordinate direction, which are assumed equal to A_h and A_v in this study. Tracers T , S , and ϕ are defined to represent temperature, salinity, and riverine tracer, respectively.

Vertical mixing is suppressed by stable stratification, so:

$$A_v = \begin{cases} 0.0004 + 6 \times 10^{-7} (N^2)^{-0.5} \text{ m}^2 \text{ s}^{-1} & N^2 > N_{\text{min}}^2 \\ 0.02 \text{ m}^2 \text{ s}^{-1} & N^2 \leq N_{\text{min}}^2 \end{cases}, \quad (6)$$

where N^2 is the stability:

$$N^2 = g\alpha \left(\frac{\partial T}{\partial z} - \Gamma \right), \quad (7)$$

which quantifies the strength of stratification such that $N^2 > 0$ for stable conditions ([Imboden and Wüest, 1995](#)). Here α is the coefficient of thermal expansion and Γ is the adiabatic temperature gradient. A cutoff value for stable conditions, $N_{\text{min}}^2 = 6.51 \times 10^{-10} \text{ s}^{-2}$, has been introduced in order to avoid large values of A_v as $N^2 \rightarrow 0$. All parameter values in this expression are chosen by fitting model results to vertical temperature profiles during the spring warming period, a procedure described by [BK](#).

Horizontal eddy viscosities are usually simply assigned a constant value, and a wide range of values is present in the literature. In this work, a value of $A_h = 2.5 \text{ m}^2 \text{ s}^{-1}$ has been adopted on the basis that it provides a reasonable thermal bar propagation rate without excessive damping of the flow field. Full details of a test of the sensitivity of model results to this parameter are given by [Holland \(2002\)](#).

Eqs. (1)–(5) are solved numerically on a staggered grid using a nonhydrostatic finite volume formulation, which employs a pressure correction procedure similar to the SIMPLE scheme of [Patankar \(1980\)](#). The computational domain is taken to be of length $L = 10$ km and depth $D = 150$ m, discretised using a uniform mesh with cell dimensions of $h_x = 25$ m by $h_z = 3$ m. A sloping delta is placed under the river inflow, as shown in [Fig. 1b](#). This gives a total of 19,010 cells, which corresponds to the maximum number of grid points that can be used with the computational resources available to this study. River inflow and outflow regions are taken to be 15-m-deep open sections at the top of the side boundaries, a choice justified fully by [Holland \(2002\)](#).

On all solid boundaries, conditions of no-slip and zero flux of scalar variables are set. At the free surface, a zero stress condition is used in conjunction with the rigid lid approximation. Radiative heating of

the lake is simulated through a thermal boundary condition at the surface, written in terms of the surface heat flux Q_s as:

$$\rho_c c_p K_v \frac{\partial T}{\partial z} = Q_s \quad (8)$$

where c_p is the specific heat at constant pressure and Q_s is measured in watts per square meter and is considered positive when entering the domain. A percentage of the solar radiation is assumed to pass through the surface to deeper regions of the lake, and the resulting heat source is assumed to have an exponential decay in intensity with depth. The vertical attenuation coefficient is taken to be 0.3 m^{-1} , as used by BK.

The river inflow and outflow are simply given a constant horizontal velocity on the open regions shown in Fig. 1b. Throughout this study, an inflow velocity of $u_R = 1 \times 10^{-2} \text{ m s}^{-1}$ is used, a value that influences the predicted flows without overpowering buoyancy effects. All scalar quantities are explicitly fixed on the inflow, but have a Neumann condition on the outflow.

All initial and boundary conditions for temperature are found from the studies of Carmack (1979) and Carmack et al. (1979). Initially, the lake has a constant temperature of $2.4 \text{ }^\circ\text{C}$, while the river is set to $3.6 \text{ }^\circ\text{C}$ in order to reproduce the measured conditions of April 8, 1975. The river is then warmed by $0.2 \text{ }^\circ\text{C day}^{-1}$ (producing a thermal bar on the third day) while a surface heat flux of $Q_s = 170 \text{ W m}^{-2}$ warms the lake throughout.

Salinity data from Kamloops Lake are relatively difficult to find, but it is clear from the small discussion of conductivity data by St. John et al. (1976) that the salinity of Kamloops Lake and the South Thompson River has a significant annual variability, peaking in late winter and troughing in the early summer freshet period. The salinities appear to be relatively homogeneous in Kamloops Lake at approximately 0.01 g kg^{-1} , and are slightly higher in the South Thompson River. For this reason, the lake is fixed to this value and the river is increased arbitrarily to test the model's sensitivity. The riverine tracer variable ϕ is introduced in order to define a mixing ratio between river and lake water, and is therefore assigned an initial value of 0 in the lake and a boundary value of 1 in the river.

3. Dynamics of the riverine thermal bar

In this section, we present results from a hydrodynamical simulation, denoted simulation *K*, which will later be used as the basis for ecological modelling studies; we also investigate the sensitivity of the present model to the various features that distinguish it from that of HKB.

The series of streamline plots in Fig. 2 shows that the nature of the thermal bar is critically dependent upon the position of the T_{md} relative to the river mouth. In the early stages of the simulation, there are steep localised temperature gradients near the inflow, generating a strong plume that sinks down the boundary (Fig. 2a). Conversely, the gentler horizontal temperature gradients present in the later stages of the model generate a weaker sinking region spread over several kilometres (Fig. 2b and c). Further studies discussed below indicate that the development of Coriolis forces may also be partly responsible for the width of this sinking region, through a weak downwards forcing inshore of the surface T_{md} .

This description of the evolution of the flow regime is supported by plots of the near-surface horizontal density profile (Fig. 3). Initially, the density variation is confined to a narrow region near the river inflow, but after 24 days significant density gradients are found in a region nearly 3 km wide inshore of the T_{md} . It can be seen that the river's density falls rapidly as the simulation proceeds, while the lake's density increases towards the maximum due to the heat flux imposed on the surface. The density profile around the thermal bar therefore evolves from a symmetric peak after 8 days to a steep one-sided density gradient after 24 days.

The rapid surface current on the inshore side of the thermal bar steadily grows in importance and is responsible for moving the T_{md} line swiftly across the lake. It can be seen that after 24 days, the lake's circulation has switched from diverting most of the river through the depths of the lake to mixing inflow water throughout the region behind the thermal bar. This is an intermediate stage in the typical spring succession, since the eventual disappearance of the thermal bar marks the onset of summer stratification and the short circuiting of warm river water across the surface of the lake (Carmack, 1979).

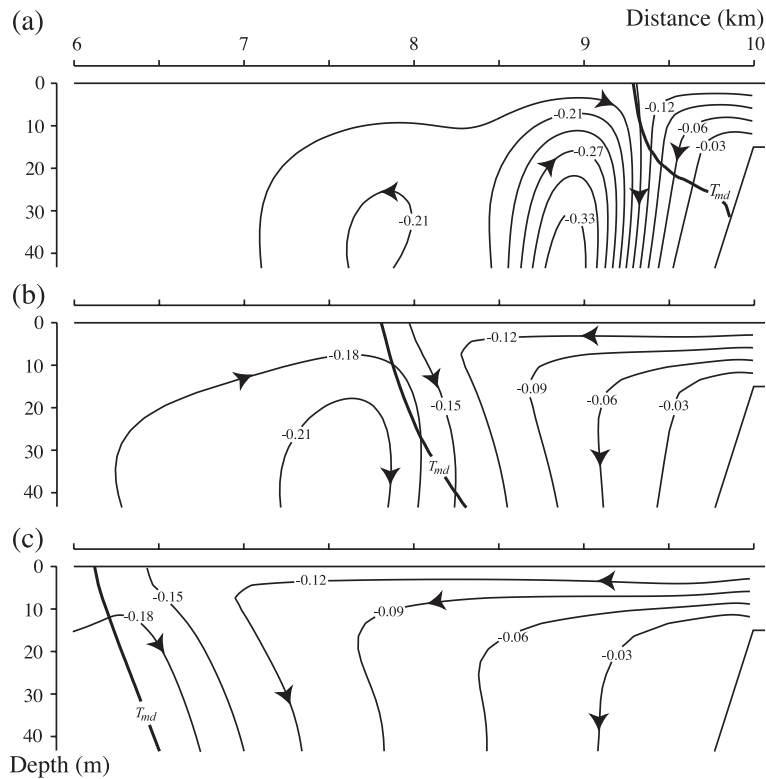


Fig. 2. Progression of the flow field throughout simulation *K*. Streamlines are marked with streamfunction values ($\text{m}^2 \text{s}^{-1}$) relative to the lake bed, and the bold line is the $T = T_{md}$ contour. (a) After 8 days: a strong plume descending near the inflow. (b) After 16 days: a weaker plume, further offshore and with downwelling in the inshore region. (c) After 24 days: a broad region of downwelling.

Fig. 4, taken from Carmack et al. (1979), shows detailed cross-sections of the temperature measurements taken on April 1, April 29, and May 8, 1975, corresponding to 8 days before the start of this

study and 20 and 30 days after. These plots show the progression from boundary current to surface overflow described above, and confirm that the dynamics of this reference simulation is at least

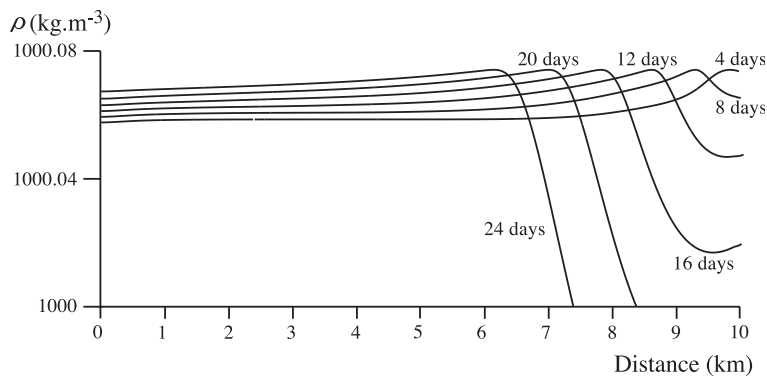


Fig. 3. Density profiles at 5 m depth throughout simulation *K*, showing the warming of the lake and the increase in inshore density gradients.

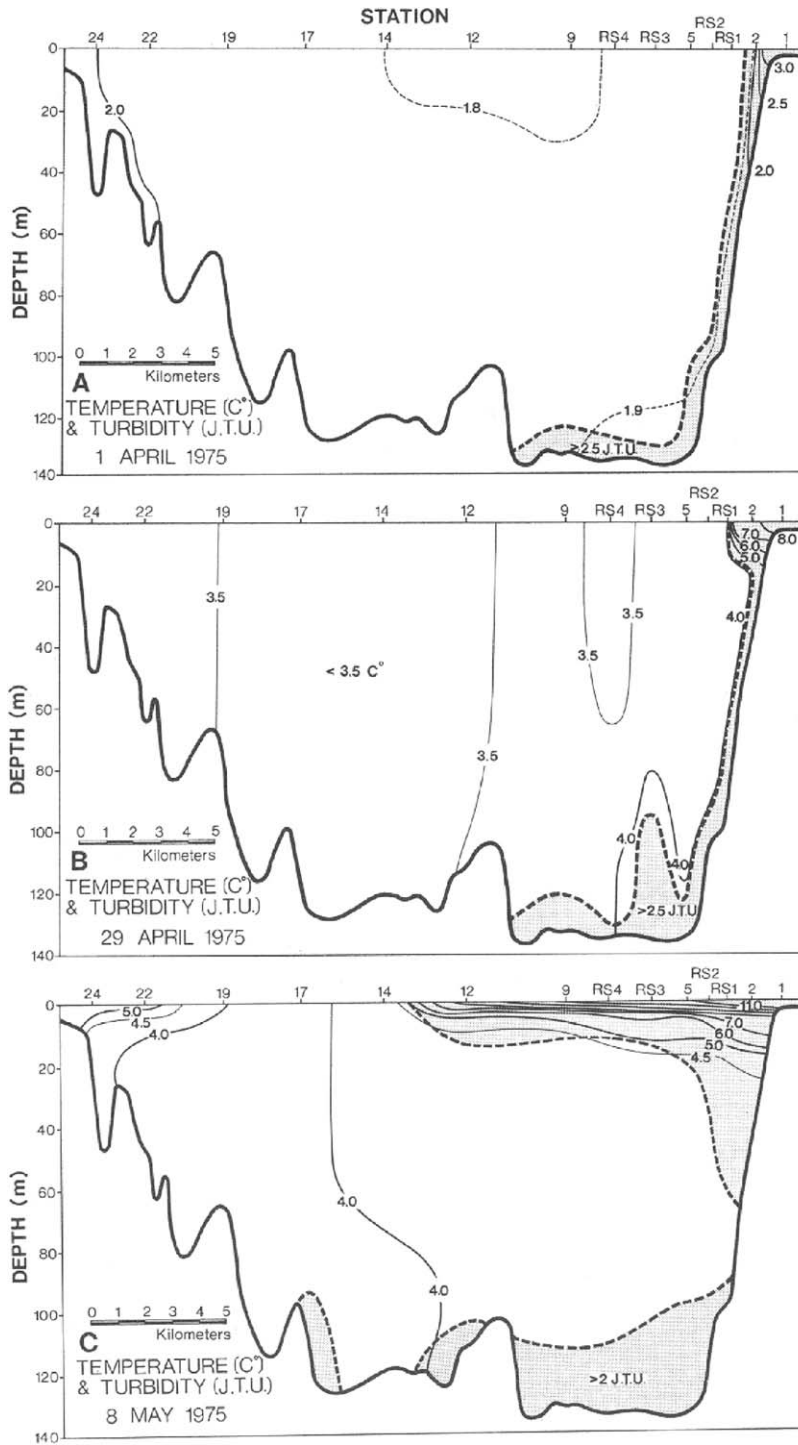


Fig. 4. Longitudinal sections of temperature and turbidity measured by Carmack et al. (1979) in Kamloops Lake during the spring thermal bar period, 1975.

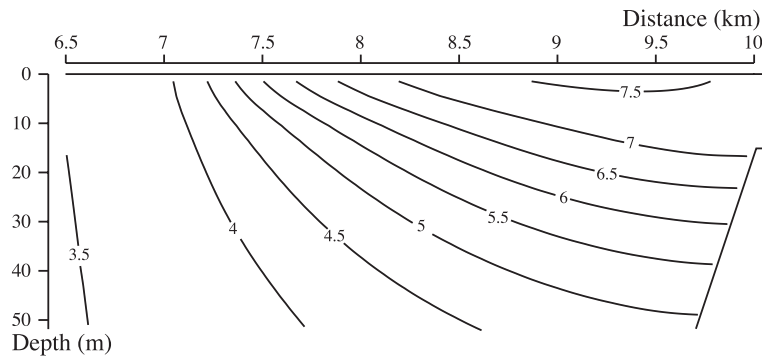


Fig. 5. Isotherms ($^{\circ}\text{C}$) in simulation *K* after 20 days: compare with the upper right-hand part of the second panel in Fig. 4.

qualitatively correct. Also, after 20 days, the thermal bar predicted by the model has propagated as far from the river inflow as that of the observations (Fig. 5). However, propagation of the model's surface gravity current 10 days later (not shown) is far too slow. This is probably due to the doubling of river discharge and large temperature increase observed in this period, features that are neglected in the model in an effort to provide a generalised thermal bar simulation.

The riverine tracer follows a straightforward progression that reflects the developing flow field of the thermal bar (Fig. 6). Tracer initially sinks down the boundary, with the vertical structure of the contours in

Fig. 6a indicating high residence times and low influence of riverine conditions on the euphotic zone. Later, the tracer spreads horizontally across the lake, with the switch to a more horizontal contour structure (Fig. 6b) heralding lower residence times and indicating that the plankton productivity in this area will eventually be heavily influenced by the riverine boundary conditions.

In the remainder of this section, we describe simulations KH, KB, and KC, in which the surface heating, sloping delta, and Coriolis force, respectively, are removed from the model. A simulation with all three removed corresponds to the model configuration of HKB, so these investigations will assess the im-

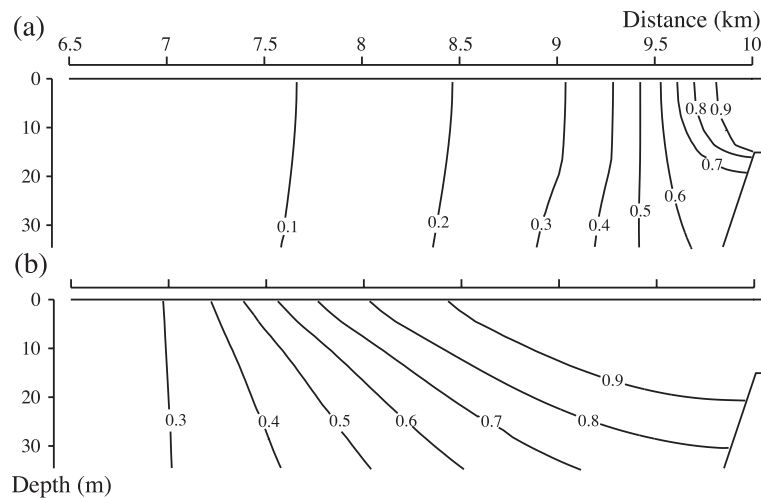


Fig. 6. Contours of riverine tracer concentration in simulation *K*, showing a progression from predominantly vertical transport (panel a, 8 days) to horizontal surface transport (panel b, 20 days).

portance of each of the improvements made to the model since the earlier paper.

An important development relative to the HKB model is the introduction of an increasing lake temperature via the surface heat flux Q_s . Fig. 3 clearly shows the increasing lake density offshore of the thermal bar, which results from a temperature increase in this region, while extra heating inshore of the T_{md} decreases the density there. In addition to simply warming more water through the T_{md} , the surface heat flux therefore quickens the development of uneven density gradients on either side of the thermal bar and hastens the progression through the flow stages discussed above.

An apparently major shortcoming of the simulations discussed in HKB is the rectangular box bathymetry employed there, which produces a cliff-like river delta and therefore casts doubt on the accuracy of the predicted transport. However, the dynamics of a Kamloops Lake simulation with the river delta slope removed (KB) is virtually identical to that of simulation K (Holland, 2002), and it is demonstrated later that the horizontal propagation rate of the T_{md} is very similar. This partly justifies the bathymetry adopted by HKB, whose need for a basic understanding of

riverine thermal bar flows limited the complexity of the domain.

A study of Coriolis forcing in this simulation is also important because the effects of the Earth's rotation were neglected by HKB. The process by which Coriolis forces affect the riverine thermal bar is explained in Fig. 7. Horizontal flow away from the river mouth inshore of the thermal bar causes a Coriolis forcing in the positive y direction (into the page in Fig. 7a), which generates a corresponding flow (Fig. 7b), in agreement with observations of a deflection to the right in the spring river plume (St. John et al., 1976; Hamblin and Carmack, 1978). The horizontal flow also leads to a negative vertical Coriolis forcing over most of the near-river region (Fig. 7c), overcoming the small positive buoyancy forcing inshore of the thermal bar and ensuring that there is a weak downwelling throughout this region rather than a recirculating cell. Finally, the x -component of Coriolis force (Fig. 7d), which is generated by the alongshore flow in Fig. 7b, has important effects on the propagation speed of the thermal bar (see below).

The most important finding of HKB is that small salinity variations may radically alter the dynamics of

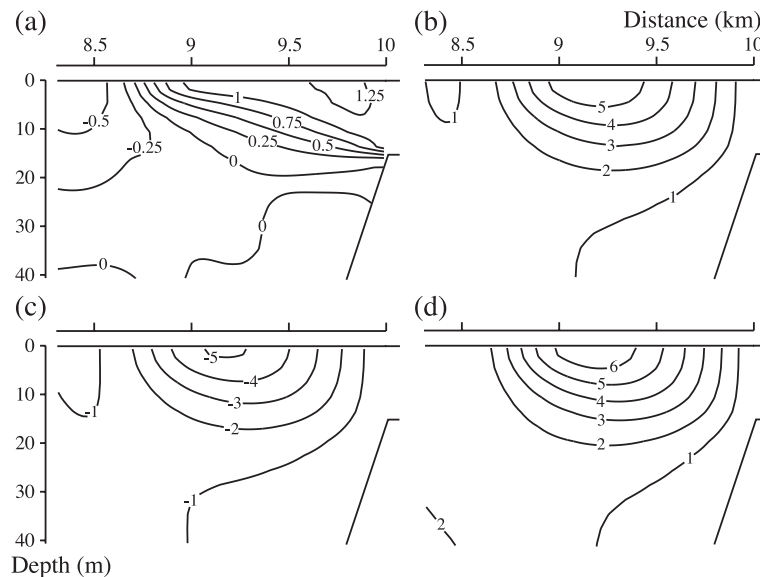


Fig. 7. Contours of Coriolis force components ($\times 10^{-6} \text{ m s}^{-2}$) and transverse velocity ($\times 10^{-2} \text{ m s}^{-1}$) in simulation K after 12 days: (a) transverse (y) component of Coriolis force; (b) consequent transverse velocity component v ; (c) vertical (z) component of Coriolis force; (d) inshore (x) component of Coriolis force.

the riverine thermal bar. The present model was tested with a range of riverine salinity increases, most of which were considerably larger than those in HKB. It is found that salinity is far less influential here because the lower lake temperature and wider range of temperatures involved in the longer time period of this study reduce the influence of salinity on the buoyancy forcing. In fact, it takes riverine salinity increases of more than 20 mg kg^{-1} to significantly affect flows.

The progression of the surface T_{md} signature is plotted in Fig. 8, which confirms that the surface heat flux plays a significant role in increasing the horizontal propagation of the thermal bar. An unexpected result is that the influence of a sloping bathymetry is rather small, highlighting the riverine dominance of thermal effects in these simulations. However, the most important feature of this horizontal progression plot is the qualitative change in thermal bar behaviour, which may be induced by the addition or neglect of Coriolis forces. Propagation of the riverine thermal bar is affected by the relative strengths of the flows converging towards it from either side. In the absence of Coriolis force, there is a strong return flow on the offshore side of the thermal bar, which retards its progression in the early stages (Holland et al., 2001), but subsequently the flow in the inshore region becomes dominant, producing the constantly accelerating propagation curve of simulation KC. However, the longitudinal (x) component of Coriolis force

always opposes the original longitudinal flow, initially weakening the offshore return flow (not shown) and subsequently impeding the inshore flow (Fig. 7d); the overall effect is to smoothen the progression to yield the near-constant velocity curve of simulation K. Note that this is a more balanced regime than that of Farrow and McDonald (2002), in which Coriolis force was so dominant that inertial oscillations occurred. In that regime, the surface convergence front (marking the centre of the downwelling plume) not only oscillates but tends to run ahead of the surface T_{md} signature. In contrast, our Fig. 2 shows the plume lagging slightly behind the T_{md} , and our Fig. 8 shows no oscillations.

The vertical tracer transport of simulations KB and KC is examined through contours of riverine tracer after 20 days of simulation, plotted in Fig. 9, which may be compared to Fig. 6b. Contours of tracer from case KH are not shown as they differ very little from those of case K, albeit with the vertical transport very slightly increased.

The results of Fig. 9a show that the rectangular box domain has a very similar distribution of tracer to case K after 20 days because the small amount of extra downwards advection predicted in this simulation has little effect upon the tracer contours. However, Fig. 9b shows that the neglect of Coriolis force causes qualitative changes in the character of the tracer distribution. The tracer is confined to a thin surface layer in case KC due to upwelling in the inshore region (Holland, 2002), but the downward Coriolis compo-

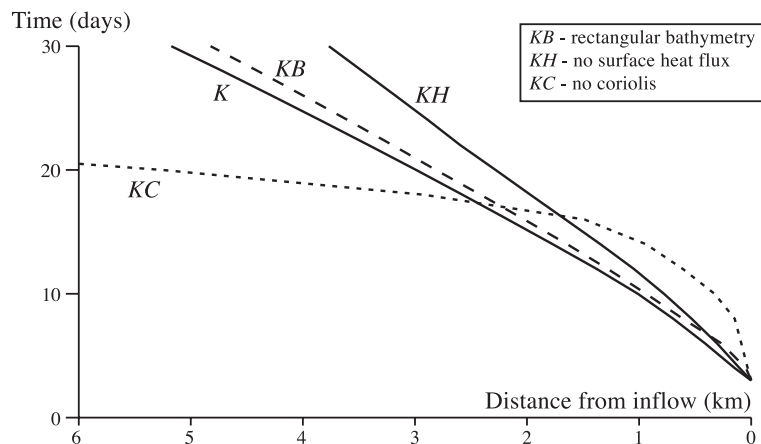


Fig. 8. Horizontal propagation of the surface T_{md} in all test cases.

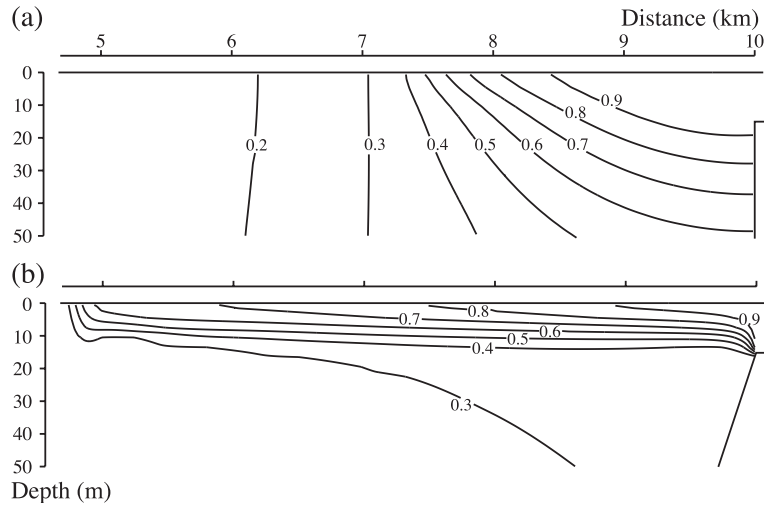


Fig. 9. Contours of riverine tracer concentration in test cases after 20 days (compare with Fig. 6b). (a) Rectangular box bathymetry, showing little change resulting from variations in basin shape. (b) Zero Coriolis forcing, resulting in reduced subsurface penetration of tracer.

ment (Fig. 7c) that suppresses this upwelling allows the tracer to penetrate to greater depths in simulation *K*. However, the more vigorous thermal bar in the Coriolis-free case does produce greater tracer concentrations at depth in the offshore region, and is more effective at mixing the tracer throughout the lake.

4. Plankton models

Biological modelling is accomplished by coupling a set of advection–diffusion equations, each governing the transport of a particular biological component, to the dynamical model described in Section 2. These equations have the following form:

$$\frac{\partial \psi}{\partial t} + u \frac{\partial \psi}{\partial x} + w \frac{\partial \psi}{\partial z} = \frac{\partial}{\partial x} \left(K_h \frac{\partial \psi}{\partial x} \right) + \frac{\partial}{\partial z} \left(K_v \frac{\partial \psi}{\partial z} \right) + S_\psi, \quad (9)$$

where ψ represents the concentration of the biological component in question (in mmol N m^{-3}) and S_ψ represents its source terms, resulting from interaction with other model components.

Two different models are used in this study: the nutrient–phytoplankton–zooplankton (*N–P–Z*) model of Franks et al. (1986) as originally adopted by BK

in a model run, which is hereafter referred to as simulation *F*, and the nutrient–phytoplankton–zooplankton–detritus (*N–P–Z–D*) model of Parker (1991), which is employed in simulation *P*.

The source terms representing the interactions between the three components of model *F* are detailed in Table 1, and all parameters associated with these terms are defined and quantified in Table 2. To enable an accurate comparison, this model is used in exactly the same form as that adopted in BK, which contains a full justification of model choices. This prevents any firm prediction of the particular plankton ecosystem of Kamloops Lake, particularly as the original Franks et al. (1986) model is conditioned for the pelagic marine ecosystem in summer, but means that important conclusions may be drawn about the differences between classical and riverine thermal bars. In any case, there are not enough data to refine the model parameters to suit the Kamloops Lake ecosystem.

Table 1
Biological interaction terms for model *F*

$$\begin{aligned} S_P &= (G - m_p)P - IZ \\ S_Z &= [(1 - \gamma)I - m_z]Z \\ S_N &= (-G + m_p)P + (\gamma I + m_z)Z \end{aligned}$$

where

$$\begin{aligned} G &= V_m e^{-\eta d} [N / (N + k_s)] \\ I &= R_m A P (1 - e^{-AP}) \end{aligned}$$

Table 2
Parameter values for model *F*

Parameter	Description	Value
V_m	Maximum phytoplankton growth rate	2.0 day^{-1}
η	Light extinction coefficient	0.1 m^{-1}
k_s	Nutrient uptake half-saturation constant	$0.2 \text{ mmol N m}^{-3}$
m_p	Phytoplankton death rate	0.1 day^{-1}
R_m	Maximum ingestion rate of zooplankton	0.5 day^{-1}
A	Ivlev constant for zooplankton grazing	$0.5 \text{ mmol N m}^{-3}$
γ	Unassimilated fraction of Z grazing	0.3
m_z	Zooplankton death rate	0.2 day^{-1}

As acknowledged by BK, the absence of temperature dependence and the phytoplankton self-shading in this simple model are significant weaknesses. In conjunction with the immediate return of plankton waste matter (mortal and fecal) to the available nutrient pool, these simplifications will tend to promote phytoplankton growth. This is rectified in simulation *P*, which accounts for temperature dependence, self-shading, and the presence of a detrital component.

The four source terms of simulation *P* are listed in Tables 3 and 4. Model *P* is adopted in precisely the same form as that of the original paper, even though some parameter values directly contradict those adopted in simulation *F*. This choice is reluctantly made due to the lack of data required to reformulate each term and fit the model's parameters. A qualitative comparison to the predictions of model *F* is still possible, however, so this model may be capable of highlighting the shortcomings of the previous formulation. This is shown in Section 7, where the results of

Table 3
Biological interaction terms for model *P*

$$\begin{aligned}
 S_p &= [(G - m_p - IZ)P]q \\
 S_z &= [(1 - \gamma_N - \gamma_D)IP - m_z Z]q \\
 S_N &= [-GP + \gamma_N IPZ + C_o D]q \\
 S_D &= [m_p P + \gamma_D IPZ - C_o D + m_z Z]q
 \end{aligned}$$

where

$$\begin{aligned}
 G &= V_m [(L_d/s_c) \exp(1 - (L_d/s_c))] [N/(N + k_s)] \\
 L_d &= L_s \exp(-\eta d - S_s \int_0^d (P + Z + D) dz) \\
 L_s &= [(75 \sqrt{2\pi}/4) N [0.5, (1/64)]] \\
 m_p &= M \exp(-(n_i N)^2) \\
 q &= 2.5^{[(T-15)/10]}
 \end{aligned}$$

Table 4
Parameter values for model *P*

Parameter	Description	Value
V_m	Maximum phytoplankton growth rate	2.8 day^{-1}
s_c	Light saturation coefficient	$60 \text{ Einstein m}^{-2} \text{ day}^{-1}$
η	Light extinction coefficient	0.15 m^{-1}
S_s	Self-shading coefficient	$0.02 \text{ (mmol N m}^{-3})^{-1} \text{ m}^{-1}$
k_s	Nutrient uptake half-saturation constant	$0.6 \text{ mmol N m}^{-3}$
I	Ingestion rate of zooplankton	0.2 day^{-1}
M	Maximum phytoplankton death rate	0.5 day^{-1}
n_i	Phytoplankton death rate coefficient	$1 \text{ (mmol N m}^{-3})^{-1}$
γ_N	Unassimilated Z grazing to nutrients	0.4
γ_D	Unassimilated Z grazing to detritus	0.3
m_z	Zooplankton death rate	0.1 day^{-1}
C_o	Detritus to nutrient conversion rate	0.02 day^{-1}

simulation *F* are qualitatively reproduced with model *P* by neglecting self-shading, temperature dependence, and detrital component.

Comparing Tables 1 and 3, it can be seen that a notable improvement of model *P* is the complexity of its photosynthesis formulation. The daily surface insolation L_s (in Einstein $\text{m}^{-2} \text{ day}^{-1}$) is assumed to have a Gaussian variation with time, which is modelled here by a normal distribution with a mean of 0.5 day and a variance of $1/64 \text{ day}^2$. This value is then adjusted so that the maximum light input is $150 \text{ Einstein m}^{-2} \text{ day}^{-1}$ at noon (Parker, 1986). The light reaching any particular depth L_d is calculated according to an exponential decay as before, but additional light depletion is included to represent self-shading by plankton and detritus in the water column between the surface ($z = F$) and $z = d$. Inhibition of growth according to the available light is then simulated using the function of Steele (1965) with a saturation coefficient s_c , which is chosen to be 40% of the noon insolation (Parker, 1991).

An important caveat to the results of this study is that neither of the Franks et al. (1986) or Parker (1991) models include gravitational sinking, which may produce different growth rates for different sizes and species of plankton (Likhoshway et al., 1996).

Also neglected is photoadaptation, whereby phytoplankton growth rates adjust to changing light availability, which may govern production under rapidly mixed conditions (Wolf and Woods, 1988). While the form of the adopted models has been chosen primarily to ease comparison, both of these effects are important under turbulent conditions and should be represented in future studies.

Selecting appropriate initial and boundary conditions for the ecological model is a major difficulty in the physical setting of a continuously interacting river and lake. The conditions chosen here are justified and discussed fully by Holland (2002). Since a comparison is sought both between the two models in this study and between this work and that of BK, initial conditions analogous to those of BK ($N-P-Z(-D)=4-1-1(-1)$ mmol N m⁻³) are adopted for both models. These choices are physically justified by the spring timing of the period of interest in this study; over winter, the plankton productivity is low in Kamloops Lake, while mortality remains roughly proportional to population levels, so that the low-biomass and nutrient-rich lake adopted here is in a theoretically suitable condition for the start of spring (St. John et al., 1976).

It is important to note that the riverine conditions of 4–1–1–1 mmol N m⁻³ adopted for the Parker (1991) model are a significant departure from the 7–0.1–0.1–0.1 mmol N m⁻³ values of the original paper. This modification is permissible, however, because the total nitrogen in the system is similar; the ecosystem is held to be in a different period of the growth cycle but generally of the same character.

Setting the riverine boundary conditions for the model is also extremely problematic, since upstream values of each component will have a very strong influence on the near-river lake region throughout the entire simulation. The preferred modelling approach would be to couple a one-dimensional river plankton model (on a vertical section) to the two-dimensional lake section and use the one-dimensional results to provide the riverine plankton levels that flow into the lake model. However, the available data fall far short of the level required to condition such models, and this approach cannot therefore be justified.

After this possibility has been ruled out, the most sensible option is to fix the values of each inflowing plankton component to a constant value throughout

the simulation. These values are chosen so that riverine component levels agree with the initial lake scenario of high nutrient levels and small plankton populations. This choice is partly made on the basis of evidence that biologically available nitrogen and phosphorus were relatively constant in the South Thompson River during April 1975 (St. John et al., 1976). Also it is well documented that plankton grow much more slowly in rivers than lakes under similar nutrient availability conditions (Jasper et al., 1983; Soballe and Kimmel, 1987). The basic assumption is therefore that the river plankton do not grow or deplete nutrients significantly for 24 days after the ecosystem starts to develop in the lake. Although this condition is clearly not realistic, it seems a more sensible choice than attempting to guess the real spring variation in riverine plankton levels.

5. Plankton populations predicted by model *F*

After 8 days of simulation, the simple three-component ecosystem model *F* is only just beginning to evolve and shows little evidence of interaction with the dynamics of the thermal bar. The phytoplankton show significant growth near the surface and a shallow maximum in the vicinity of the thermal bar (Fig. 10a), but the zooplankton hardly react at all with the other components of the plankton model, their distribution being determined almost entirely by mortality and the riverine boundary conditions (Fig. 10b).

In the interest of brevity, the concentration of plankton model components will hereafter be shown as horizontal profiles from a depth of 5 m. Fig. 11a, an example of this, shows that the phytoplankton have taken up more nitrogen than is depleted from the nutrient pool, indicating that zooplankton mortality and the river inflow are maintaining available nutrient levels.

After 16 days of simulation, the thermal bar has progressed much further from the inflow (Fig. 2b), and phytoplankton growth at the position of the thermal bar has reached bloom levels (Fig. 11b). Zooplankton concentrations also reach a shallow maximum at the thermal bar, but it is clear that transport of riverine zooplankton is more important overall than in situ growth. The nutrient pool near the

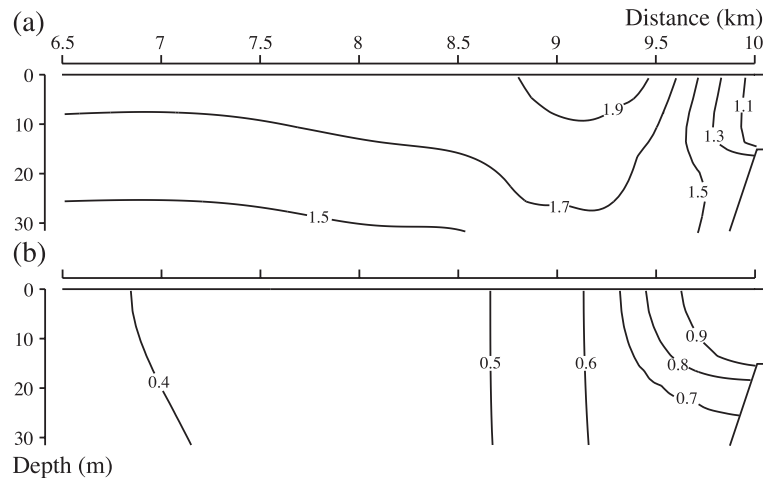


Fig. 10. Contours of ecological model components (mmol N m^{-3}) in simulation *F* after 8 days: (a) phytoplankton, showing a shallow surface maximum around the thermal bar; (b) zooplankton, showing depletion by mortality away from the river inflow.

thermal bar is greatly reduced by the phytoplankton bloom and drops to a level that will restrict any further production (Holland, 2002).

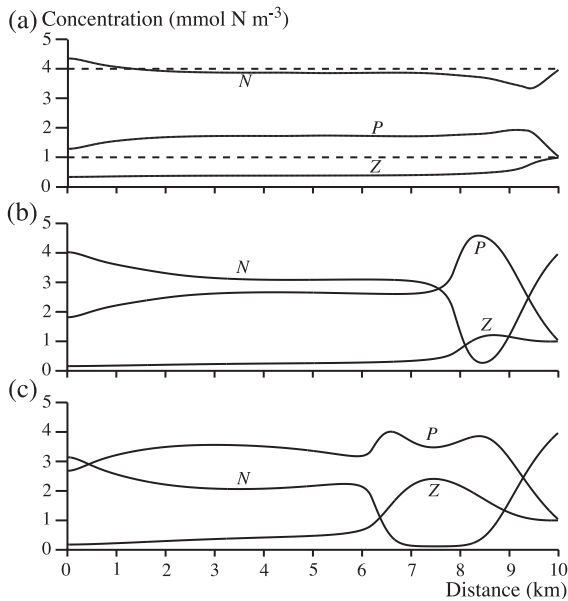


Fig. 11. Horizontal profiles of all components in simulation *P* at 5 m depth, with broken lines indicating initial conditions. (a) After 8 days (as Fig. 10). (b) After 16 days: phytoplankton bloom and severe nutrient depletion around the thermal bar. (c) After 24 days: double phytoplankton bloom, related to nutrient depletion and zooplankton grazing.

After 24 days of simulation, the phytoplankton are concentrated into two distinct blooms of similar magnitude: one at the position of the thermal bar and the other midway between the thermal bar and the river inflow (Fig. 11c). The main cause of this unusual distribution is nutrient limitation: the nutrient minimum resulting from the earlier bloom (Fig. 11b) impedes further growth in this location, but phytoplankton can continue to grow unrestricted in the higher nutrient levels on either side. As the thermal bar propagates, it leaves a large region in its wake, which contains virtually no available nutrients.

Fig. 11c shows that the main zooplankton growth takes place between the two phytoplankton blooms, indicating that zooplankton grazing may also contribute to the double-bloom structure, although its role is difficult to quantify. A close examination of the Michaelis–Menten factor in the photosynthesis formulation (Table 1) confirms that nutrient limitation must be responsible for initiating the depression in the centre of the original phytoplankton bloom. Nevertheless, zooplankton grazing terms significantly deplete phytoplankton concentrations in the region between the two blooms throughout the later stages of the simulation (Holland, 2002).

An important conclusion of BK is that the productivity of a plankton ecosystem is fundamentally dependent upon water column stability, which can delay the diffusion of phytoplankton downwards from the

highly productive euphotic zone near the lake surface. Contours of N^2 after 20 days of simulation are shown in Fig. 12, and may be compared with those for a radiatively forced thermal bar in BK's Fig. 10. In both cases, the thermal bar acts as a boundary between stable and unstable water columns. However, whereas stability increases monotonically towards the surface in the region inshore of BK's thermal bar, the riverine case has a sloping subsurface stability maximum due to the thermocline formed by the base of the well-mixed river overflow. This high-stability layer intersects the surface between the vertically well-mixed regions at the river inflow and at the thermal bar, which have relatively low stability.

Comparing vertical $N-P-Z$ profiles to contours of stability in Fig. 12 shows that plankton development offshore of the thermal bar (6.5 km from the origin) is clearly limited by diffusion of the photosynthesising phytoplankton downwards, whereas growth at the surface stability maximum inshore of the T_{md} (8.25

km from the origin) continues until the water is almost completely devoid of nutrients. Overall plankton growth is also more prolific in the stable regions inshore of the T_{md} than it is at the stagnation point above the thermal bar plume (7.25 km from the origin), although at the stage shown in Fig. 12 zooplankton have grazed the excess phytoplankton in the inshore region so that the difference is only apparent in the Z component and in nutrient depletion. Thus, stability is more influential than the converging horizontal transport at the surface T_{md} or the low-plankton riverine boundary conditions, although the latter combines with the subsurface stability maximum to produce the $N-P-Z$ profiles at 9.25 km from the origin.

In contrast to the 'bloom and bust' character of the phytoplankton predicted by this model, St. John et al. (1976) observed that phytoplankton populations in Kamloops Lake continue to develop steadily throughout spring and into late summer. Our prediction of a

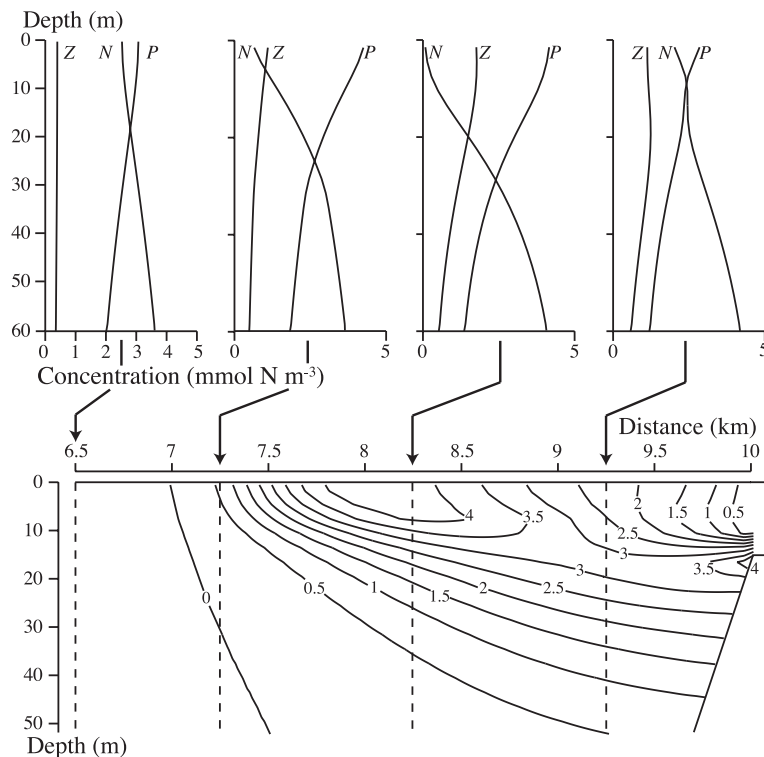


Fig. 12. Contours of static stability N^2 (s^{-2}) and vertical profiles of the three components of model F , showing that plankton productivity is maximised when near-surface stability is greatest.

double phytoplankton bloom after only 24 days lies in contradiction to these (admittedly sparse) observations, leading to a suspicion that it may result from a deficiency in the model's representation of the ecosystem. In adopting the Franks et al. (1986) model, BK argued that its growth rates were not ideally suited to modelling temperate lake plankton in spring due to the lack of any temperature dependence. When the absence of self-shading and the immediate return of detritus to the available nutrient pool are also considered, it is clear that the main simplifications of this model all tend to produce higher productivity than would otherwise be the case. The extent to which this model oversimplification can be rectified realistically and at reasonable computational expense is explored in Section 6 by a discussion of the results of the N – P – Z – D ecosystem model of Parker (1991), which is coupled to the same Kamloops Lake dynamics.

6. Plankton populations predicted by model P

After only 8 days of simulation, it is obvious from phytoplankton concentrations that simulation P will produce a totally different ecosystem to simulation F (Fig. 13a). Phytoplankton growth is less prolific in this model and is restricted to the near-river region, appearing to be dominated by the inflow boundary conditions. This distribution is actually supported by photosynthesis, as the temperature dependence favours growth in the warm river region rather than at the T_{md} (Holland, 2002). The halving of zooplankton mortality compared to the Franks et al. (1986) formulation overcomes the generally lower assimilated grazing rate and allows far more zooplankton to survive.

The phytoplankton bloom that emerges after 16 days has a much smaller magnitude than that of simulation F (compare Figs. 11b and 13b), and is localised closer to the river at the stability maximum inshore of the surface T_{md} . As illustrated by later analyses, this is caused by the temperature dependence skewing phytoplankton growth towards the warm river. There is still little sign of any zooplankton growth independently of the riverine boundary conditions.

After 24 days, the predictions of phytoplankton concentration in models P and F are qualitatively different. While simulation F now has a fully devel-

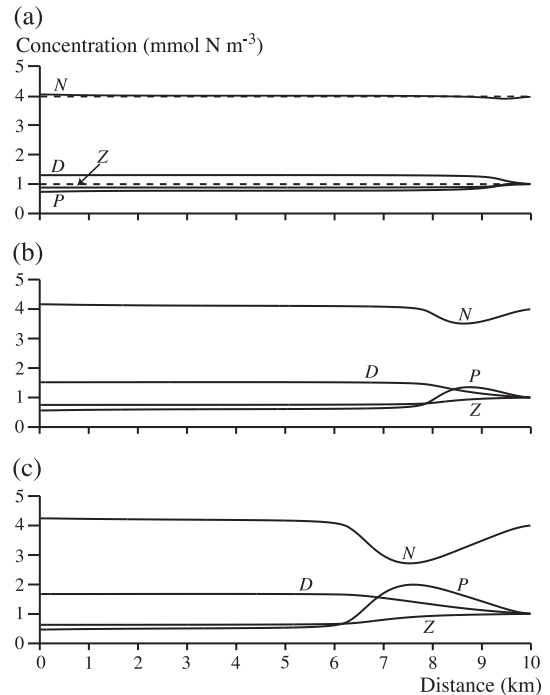


Fig. 13. Horizontal profiles of all components in simulation P at 5 m depth. (a) After 8 days: all components are dominated by riverine boundary conditions. (b) After 16 days: incipient phytoplankton bloom inshore of thermal bar. (c) After 24 days: more developed phytoplankton bloom, but zooplankton still controlled by river conditions.

oped double phytoplankton bloom, simulation P still shows a single bloom, inshore of the T_{md} and with maximum phytoplankton concentrations at a value of half of that attained by simulation F after only 16 days (Fig. 13c). As with the earlier stages of simulation, zooplankton distributions are still dominated by riverine effects after 24 days of open-lake grazing, showing a gradual decline away from the river plume region in contrast to the zooplankton bloom of simulation F .

The most important difference between simulations P and F is in the photosynthesis rate. In particular, simulation P restricts the majority of phytoplankton growth to the near-river areas, whereas a fair amount of photosynthesis takes place offshore of the T_{md} in simulation F . This happens because temperature dependence favours biological interaction near the warm river inflow, resulting in the situation pictured in Fig. 13c.

As a result of the stunted phytoplankton growth in the open lake, nutrient levels stay fairly constant there throughout simulation *P* despite the delay in returning planktonic detritus to the nutrient pool. This result is contrary to the observations of simulation *F*, where nutrients are rapidly depleted everywhere under the pressure of mass phytoplankton growth. Of all components, it is the detritus which gains the most nitrogen when averaged over the whole open lake because plankton mortality and unassimilated zooplankton grazing exceed the detritus-to-nutrient conversion rate.

A closer examination of the magnitude of terms in the zooplankton equation reveals the dominance of transport processes over the biological production and destruction of zooplankton (Holland, 2002). This explains the observations that zooplankton concentrations are dominated by the riverine boundary conditions throughout simulation *P*.

7. The influence of model *P* features

The qualitative differences between the plankton predictions of each model lead to the question of why these simple models should give such vastly different answers in the same dynamical and thermal regime. A thorough comparison of the two models requires an assessment of the contribution of each of the five major differences between the model formulations. It is found that the phytoplankton mortality and zooplankton grazing terms are relatively unimportant (Holland, 2002), so we proceed by considering the influence of the remaining factors: detritus, temperature dependence, and self-shading. Simulations with each of these factors removed in turn are referred to as PD, PT, and PS, respectively. In addition, simulation PTSD has all three of these features neglected.

It can be seen from the results of simulation PD after 24 days (Fig. 14) that removing the detritus component of simulation *P* actually has very little effect on the plankton ecosystem. Nutrient levels are increased by the same amount that detritus gained previously, as all plankton waste products are now returned directly to the nutrient pool, but this prompts only a minor reduction in nutrient limitation and does not lead to a noticeable increase in plankton. This result is in full agreement with the findings of

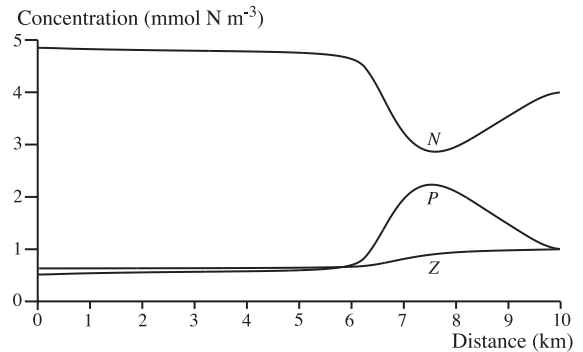


Fig. 14. Horizontal profile of all components in simulation PD at 5 m depth after 24 days, showing the main effect of removing the detritus component to be an equivalent increase in nutrients (compare with Fig. 13c).

Edwards (2001), who showed that the inclusion of detritus only affects a model's behaviour significantly when zooplankton are allowed to graze it.

The removal of phytoplankton self-shading has a more significant effect on the ecosystem (Fig. 15). The obvious consequence of this step is an increase in photosynthesis, and comparing the *N–P–Z–D* profiles in Figs. 13c and 15 shows that simulation PS has a doubled net phytoplankton growth over the first 24 days of simulation.

Ignoring the temperature dependence of the Parker model has a far more profound effect on the ecosystem predictions than either of the two previous changes. As simulation PT was performed by fixing *q* to be constant at a value corresponding to the Franks et al. (1986) formulation ($T=20\text{ }^{\circ}\text{C}$), the effects of this step are to remove the preference for growth in the warm river inflow and to generally increase the rate of all biological interactions. Fig. 16 shows that the effect of standardising *q* is to increase the phytoplankton production and to promote photosynthesis over a much wider area, including offshore of the T_{md} . This extra growth may not seem obvious from a comparison of the plankton components in Figs. 13c and 16, but must have occurred because the detritus component is substantially greater as the increased mortality rates have transferred the plankton biomass to detritus.

None of the variant simulations above seems to be much closer to simulation *F* than simulation *P*, but the progression of simulation PTSD (Fig. 17) shows

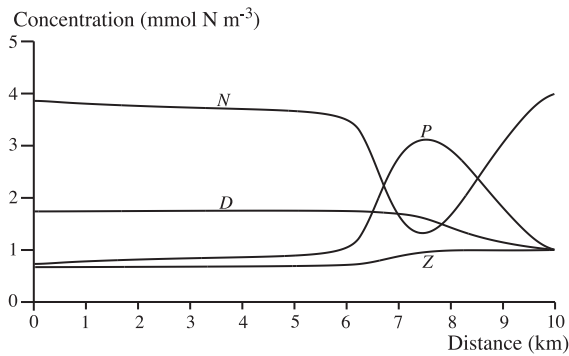


Fig. 15. Horizontal profile of all components in simulation PS at 5 m depth after 24 days, showing the increased phytoplankton growth when self-shading is eliminated (compare Fig. 13c).

results that are remarkably similar to those of Fig. 11. All the qualitative features of simulation *F* are reproduced by simulation PTSD after 24 days, except that the double-bloom structure is not fully developed until day 30. This delay, and the broader form of the eventual double bloom in simulation PTSD, are due to the smoother impedance of photosynthesis by nutrient limitation, as quantified by the higher value of k_s ; also, the nutrients themselves are not depleted so drastically. Furthermore, the zooplankton grazing rate is much lower in simulation *P*, which explains the generally lower zooplankton levels in all *P* variants as well as lessening the influence of zooplankton on the double-bloom formation.

Considering the differences in formulation and parameter values that are still present between simu-

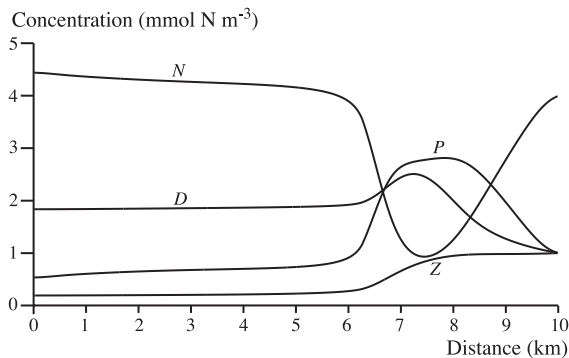


Fig. 16. Horizontal profile of all components in simulation PT at 5 m depth after 24 days, showing a broader phytoplankton bloom and increased detritus resulting from biological interactions at rates appropriate to $T=20$ °C (compare with Fig. 13c).

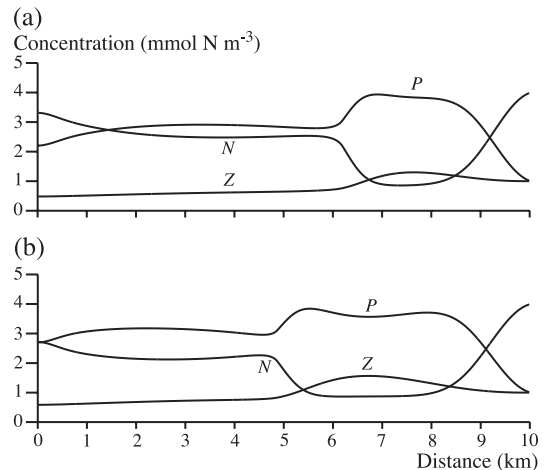


Fig. 17. Horizontal profiles of all components in simulation PTSD at 5 m depth. (a) After 24 days: a broad phytoplankton bloom and incipient zooplankton growth, with significant nutrient depletion. (b) After 30 days: double-bloom structure appears (compare with Fig. 11c).

lations *F* and PTSD, it is very interesting that this simplified version of simulation *P* is able to qualitatively reproduce the results of Section 5. To quantitatively reproduce simulation *F* from the basis of the Parker (1991) model, it would probably only be necessary to further alter the nutrient limitation factor and zooplankton growth and mortality rates.

8. Discussion and conclusions

We consider our results in comparison to previous related studies. Firstly, the hydrodynamical results are compared to the deep-lake simulations of HKB; then the ecological results are compared to the findings of BK for a radiatively forced thermal bar.

We have found that the hydrodynamical model is capable of qualitatively reproducing the riverine thermal bar observations of Carmack et al. (1979) and is therefore a reasonable basis for the ecological study. This is the first time the riverine thermal bar has been successfully modelled throughout the spring warming period, and provides a greater insight into its behaviour than the rather idealised model of HKB. However, revealing tests of the sensitivity of the riverine thermal bar to salinity and Coriolis force broadly support the assumptions made in the deep-lake model of HKB.

In contrast to that work, it is found that the spring riverine thermal bar of Kamloops Lake is unresponsive to all reasonable increases in riverine salinity. This relates to the much greater temperature variations and the longer period of the Kamloops Lake model run: offshore, the difference from T_{md} is initially set to 1.6 °C in Kamloops but less than 0.4 °C in the deep lake, while inshore temperature differences from T_{md} after 24 days of the Kamloops model run are about twice the maximum inshore difference of 2 °C found in the deep-lake model. Thus, a comparison of the two models provides a useful measure of the relative importance of thermal and haline contributions to buoyancy forcing in thermal bar situations.

It is confirmed here that Coriolis forces play an extremely important role in the development of the riverine thermal bar. Nevertheless, the neglect of Coriolis effects in the deep lake of HKB is justified by the short timespan of those simulations: there is an initial spin-up period, during which the Coriolis force establishes a flow in the y -direction, which then proceeds to modify the thermal bar dynamics. If Coriolis force had been included in the deep-lake model, only the spin-up would have been observed in the simulations. A realistic assessment of Coriolis effects requires the longer period of the Kamloops simulation.

The effects of other features neglected by HKB, surface heating and bathymetry, are shown to be much less important, with a simulation corresponding to the conditions of HKB noting only a slight decrease in horizontal transport. Overall, the present study gives no reasons to reject the basic findings of HKB for the limited timespan considered therein, but a longer-period deep-lake study that would be possible with greater computational resources would also require the extra sophistication of the Kamloops Lake model. Further worthwhile improvements would include:

extending to three dimensions to fully capture Coriolis and bathymetric effects; adopting a higher-order turbulence closure to fully elucidate the effects of river plume mixing; and modelling the entire annual cycle of a river-dominated temperate lake, thus including an examination of the poorly understood autumn riverine thermal bar.

Whereas there is a sufficient body of field data to enable meaningful validation of model results relating to the hydrodynamics of Kamloops Lake, data on the lake's plankton ecology are very sparse. Hence, while our ecological modelling can provide qualitative comparisons between plankton population dynamics in BK's 'classical' thermal bar (for which a reasonable fit was obtained to plankton data from Lake Baikal by Likhoshway et al., 1996) and the riverine thermal bar of this study, and also between different ecological model formulations, it cannot yield quantitative predictions for any particular lake.

Comparing plankton concentrations after 16 days of simulation F (Fig. 18) with those after 20 days from BK's simulation using an identical version of the Franks et al. (1986) model (BK's Fig. 12), it is clear that the rate of phytoplankton growth is significantly greater in the riverine simulation. Further confirmation of this is that the double phytoplankton bloom has not appeared even after 40 days of BK's simulation, although a double peak in primary production has just appeared at that stage (BK's Fig. 16). As all model parameters are the same in each study, there are only two broad potential causes for this: the lake's thermal regime and the influence of the plankton riverine boundary conditions. Previous work on the effects of stability indicates that it is the stability-led differences in vertical diffusivity which lead to the differences in growth rate, rather than the effects of the fixed boundary plankton levels (Holland, 2002). In addition, ver-

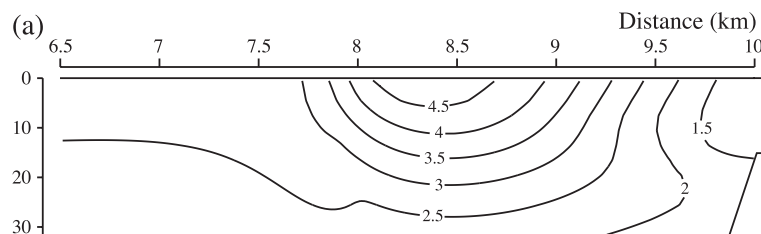


Fig. 18. Contours of phytoplankton concentration (mmol N m^{-3}) predicted by simulation F after 16 days, showing greater growth rates than in BK's deep-lake model.

tical N – P – Z variations are shown to be strongly correlated with stability profiles, and N^2 values are generally several orders of magnitude higher in simulation F than in BK. Therefore, we conclude that the riverine thermal bar supports plankton growth better than a nonriverine thermal bar because of the stability structure induced by a river inflow.

It is reasonable to assume that a strong enough river inflow could cause enough turbulence in the near-shore region to offset these effects of stability on the plankton growth. As the neglect of shear effects in the vertical eddy viscosity is fully justified by Holland (2002), the possible consequences of this effect are disregarded here. Nevertheless, improvements to the turbulence model are probably necessary to properly describe the effects of river-generated turbulence and their influence on plankton populations.

It is important to note that, in the absence of any high-resolution data on the spring phytoplankton bloom in Kamloops Lake, it is impossible to conclusively say which of the two models produces the most reasonable approximation to real plankton populations. Although it has been shown that the ‘double-bloom’ predictions from the model of Franks et al. (1986) are not found in a more sophisticated model, there is no certain way of knowing whether the latter is a more appropriate formulation for Kamloops Lake in the spring. However, it is noted here that the Parker (1991) model predicts photosynthesis rates that generally agree with a steady productivity over several months, as observed in Kamloops Lake by St. John et al. (1976). It is therefore thought that growth is probably excessive in simulation F since the Franks et al. (1986) model is conditioned to the marine pelagic ecosystem in summer and there are no reports of a ‘double bloom’ in phytoplankton in temperate lakes in spring. By experimentation with the more complex model (which admittedly is also conditioned for summer marine waters), it was shown that the double-bloom results may only be reproduced by ignoring all three of its most significant facets at the same time. The removal of temperature dependence and self-shading simultaneously allows a large increase in photosynthesis and a shift of phytoplankton growth away from the river inflow (not shown), and the removal of the detritus component then ensures that nutrient limitation acts in exactly the manner required for the prediction of a double bloom. This

supports the contention that the double bloom is probably due to the excessive phytoplankton growth, which results from oversimplifications in the Franks et al. (1986) model, since it takes a particular combination of three clearly unphysical assumptions to produce this phenomenon.

In summary, our ecological modelling has shown that a riverine thermal bar promotes plankton growth more strongly than a radiatively forced thermal bar, and has elucidated the effects of detritus, self-shading, and temperature dependence on simple plankton formulations. Each of the latter factors can clearly produce qualitative differences in the predictions of a plankton model, so they should be included whenever an application includes sufficient data for parameter fitting. A great deal of useful information may be gained from a very simple plankton model, as shown by BK, but this study concludes that such results should only be applied with great caution.

Acknowledgements

This work was funded by the UK Natural Environment Research Council under grant no. GR3/11029.

References

- Botte, V., Kay, A., 2000. A numerical study of plankton population dynamics in a deep lake during the passage of the Spring thermal bar. *J. Mar. Syst.* 26, 367–386.
- Brooks, I., Lick, W., 1972. Lake currents associated with the thermal bar. *J. Geophys. Res.* 77, 6000–6013.
- Budd, J., Kerfoot, W.C., Pilant, A., Jipping, L.M., 1999. The Keeweenaw current and ice rafting: use of satellite imagery to investigate copper-rich particle dispersal. *J. Great Lakes Res.* 25, 642–662.
- Carmack, E.C., 1979. Combined influence of inflow and lake temperatures on Spring circulation in a riverine lake. *J. Phys. Oceanogr.* 9, 422–434.
- Carmack, E.C., Gray, C.B.J., Pharo, C.H., Daley, R.J., 1979. Importance of lake–river interaction on seasonal patterns in the general circulation of Kamloops Lake, British Columbia. *Limnol. Oceanogr.* 24, 634–644.
- Chen, C.T.A., Millero, F.J., 1986. Precise thermodynamic properties for natural waters covering only the limnological range. *Limnol. Oceanogr.* 31, 657–662.
- Edwards, A.M., 2001. Adding detritus to a nutrient–phytoplankton–zooplankton model: a dynamical-systems approach. *J. Plankton Res.* 23, 389–413.

- Farrow, D.E., McDonald, N.R., 2002. Coriolis effects and the thermal bar. *J. Geophys. Res.* 107, 1–9.
- Franks, P.J.S., Wroblewski, J.S., Flierl, G.R., 1986. Behaviour of a simple plankton model with food-level acclimation by herbivores. *Mar. Biol.* 91, 121–129.
- Gbah, M.B., Murthy, R.C., 1998. Characteristics of turbulent cross and along-shore momentum exchanges during a thermal bar episode in Lake Ontario. *Nord. Hydrol.* 29, 57–72.
- Gray, C.B.J., Tuominen, T.M. (Eds.), 1999. Health of the Fraser River Aquatic Ecosystem: A Synthesis of Research Conducted Under the Fraser River Action Plan. Environment Canada, Vancouver, BC, Canada. DOE FRAP 1998-11.
- Hamblin, P.F., Carmack, E.C., 1978. River-induced currents in a fjord lake. *J. Geophys. Res.* 83, 885–899.
- Holland, P.R., 2002. Numerical modelling of the riverine thermal bar. PhD Thesis, Loughborough University, UK. Unpublished.
- Holland, P.R., Kay, A., Botte, V., 2001. A numerical study of the dynamics of the riverine thermal bar in a deep lake. *Environ. Fluid Mech.* 1, 311–332.
- Huang, J.C.K., 1972. The thermal bar. *Geophys. Fluid Dyn.* 3, 1–25.
- Imboden, D.M., Wüest, A., 1995. Mixing mechanisms in lakes. In: Lerman, A., Imboden, D., Gat, J. (Eds.), *Physics and Chemistry of Lakes*. Springer-Verlag, Berlin, pp. 83–138.
- Jasper, S., Carmack, E.C., Daley, R.J., Gray, C.B.J., Pharo, C.H., Wiegand, R.C., 1983. Primary productivity in a large, temperate lake with river interflow: Kootenay Lake, British Columbia. *Can. J. Fish. Aquat. Sci.* 40, 319–327.
- Killworth, P.D., Carmack, E.C., 1979. A filling-box model of river-dominated lakes. *Limnol. Oceanogr.* 24, 201–217.
- Likhoshway, Y.V., Kuzmina, A.Ye., Potyemkina, T.G., Potyemkin, V.L., Shimaraev, M.N., 1996. The distribution of diatoms near a thermal bar in Lake Baikal. *J. Great Lakes Res.* 22, 5–14.
- Moll, R.A., Bratkovitch, A., Chang, W.Y.B., Pu, P., 1993. Physical, chemical, and biological conditions associated with the early stages of the Lake Michigan vernal thermal front. *Estuaries* 16, 92–103.
- Parker, R.A., 1986. Simulating the development of Chlorophyll maxima in the Celtic Sea. *Ecol. Model.* 33, 1–11.
- Parker, R.A., 1991. Eddy diffusion of phytoplankton and nutrients: estimating coefficients from simulated and observed vertical distributions. *J. Plankton Res.* 13, 815–830.
- Patankar, S.V., 1980. *Numerical Heat Transfer and Fluid Flow*. Hemisphere, New York.
- Soballe, D.M., Kimmel, B.L., 1987. A large-scale comparison of factors influencing phytoplankton abundance in rivers, lakes, and impoundments. *Ecology* 68, 1943–1954.
- Steele, J.H., 1965. Notes on some theoretical problems in production ecology. *Mem. Ist. Ital. Idrobiol. Dr. Marco De Marchi* 18, 383–398 (Supplement).
- St. John, B.E., Carmack, E.C., Daley, R.J., Gray, C.B.J., Pharo, C.H., 1976. The Limnology of Kamloops Lake, British Columbia. Inland Waters Directorate, Vancouver, BC, Canada.
- Ullman, D., Brown, J., Cornillon, P., Mavor, T., 1998. Surface temperature fronts in the Great Lakes. *J. Great Lakes Res.* 24, 753–775.
- Ward, F.J., 1964. Limnology of Kamloops Lake. Bulletin, vol. XVI. International Pacific Salmon Fisheries Commission, New Westminster, BC, Canada.
- Wolf, K.U., Woods, J.D., 1988. Lagrangian simulation of primary production in the physical environment—the deep chlorophyll maximum and nutricline. In: Rotschild, B.J. (Ed.), *Toward a Theory of Biological–Physical Interaction in the World Ocean*. Kluwer, Dordrecht, pp. 51–70.
- Zilitinkevich, S.S., Kreiman, K.D., Terzhevik, A.Yu., 1992. The thermal bar. *J. Fluid Mech.* 236, 22–47.